Title

Maximum time-resolved hemispherical reflectance of absorbing and isotropically scattering media

Journal

Journal of Quantitative Spectroscopy & Radiative Transfer, 104(3)

ISSN

0022-4073

Authors

Smith, K D
Katika, K M
Pilon, L

Publication Date

2007-04-01

Peer reviewed

Maximum Time-Resolved Hemispherical Reflectance of Absorbing and Isotropically Scattering Media

Kyle D. Smith, Kamal M. Katika, and Laurent Pilon

Mechanical and Aerospace Engineering Department
420 Westwood Plaza, 37-132 Eng. IV
Henri Samueli School of Engineering and Applied Science
University of California, Los Angeles - Los Angeles, CA 90095, USA
Phone: +1 (310)-206-5598, Fax: +1 (310)-206-2302
E-mail: pilon@seas.ucla.edu

Abstract

This paper presents a parametric study of the time-resolved hemispherical reflectance of a plane-parallel slab of homogeneous, cold, absorbing, and isotropically scattering medium exposed to a collimated Gaussian pulse. The front surface of the slab is transparent while the back surface is assumed to be cold and black. The one-dimensional time-dependent radiation transfer equation is solved using the modified method of characteristics. The parameters explored include (1) the optical thickness, (2) the single scattering albedo of the medium, and (3) the incident pulse width. The study pays particular attention to the maximum transient hemispherical reflectance and identifies optically thin and thick regimes. It shows that the maximum reflectance is independent of the optical thickness in the optically thick regime. In the optically thin regime, however, the maximum hemispherical reflectance depends on all three parameters explored. The transition between the optically thick and thin regimes occurs when the optical thickness is approximately equal to the dimensionless pulse width. Finally, correlations relating the maximum of the hemispherical reflectance as a function of the optical thickness, the single scattering albedo of the materials and the incident pulse width have been developed. These correlations could be used to retrieve radiation characteristics or serve as initial guesses for more complex inversion schemes accounting for anisotropic scattering.

Key words: transient radiative transfer, method of characteristics, scattering, turbid media, tomography, biological tissues.

1 INTRODUCTION

Transient radiation transfer has found numerous applications in (1) laser-assisted micromachining, (2) remote sensing of combustion systems, and (3) of biological tissues among others [1]. The governing equation for radiation transfer in homogeneous, absorbing, emitting, and scattering media is the so-called radiative transfer equation (RTE). It expresses an energy balance in a unit solid angle $d\Omega$ about the direction $\hat{\mathbf{s}}$. For a non-emitting medium, on a gray basis, it can be written as [2],

$$\frac{1}{c}\frac{\partial I}{\partial t} + (\hat{\mathbf{s}} \cdot \nabla) I = -\kappa I - \sigma_s I + \frac{\sigma_s}{4\pi} \int_{4\pi} I(\hat{\mathbf{s}}_i) \Phi(\hat{\mathbf{s}}_i, \hat{\mathbf{s}}) \mathrm{d}\Omega_i \tag{1}$$

where I is the intensity in the $\hat{\mathbf{s}}$-direction and c is the speed of light in the medium. The linear absorption and scattering coefficients are denoted by κ and σ_s, respectively. The first and second terms on the right-hand side of the equation represent attenuation of radiation by absorption and scattering, respectively. Finally, the last term on the right-hand side corresponds to the augmentation of radiation due to in-scattering. The scattering phase function $\Phi(\hat{\mathbf{s}}_i, \hat{\mathbf{s}})$ represents the probability that radiation propagating in the solid angle $\mathrm{d}\Omega_i$ around direction $\hat{\mathbf{s}}_i$ will be scattered into the cone $\mathrm{d}\Omega$ around the direction $\hat{\mathbf{s}}$. The transient RTE is an integro-differential equation involving seven independent variables. In addition, various other factors like geometry, temperature fields, and the radiation characteristics of the medium make the RTE difficult to solve.

Established techniques for estimating the absorption and scattering coefficients as well as the scattering phase function consist of measuring the spectral or total, directional-hemispherical or directional-directional transmittance and reflectance, with collimated or diffuse incident radiation. First, initial values for the radiation characteristics are assumed and the RTE is solved. The calculated and measured quantities are compared and a new estimate of the radiation characteristics is made. This procedure is accomplished in an iterative and time consuming manner until the set of absorption and scattering coefficients and scattering phase function minimizes the difference between the measured and the calculated properties. The major difficulty inherent to the inverse method is that there is no unique solution for the radiation characteristics. Moreover, due to the iterative nature of the method, the initial guess for radiation characteristics are of major importance if one wants a rapid convergence toward the optimum solution.

Moreover, Yamada and Kurosaki [3] retrieved the radiation characteristics of porous materials from emittance measurements. Indeed, the authors assumed an isotropic scattering phase function and used the fact that the emittance of

an optically thick and isotropically scattering medium is independent of the optical thickness and depends only on the single scattering albedo. Finally, they recommended their method for highly scattering media rather than for absorbing media since the albedo is very sensitive to emittance and that the latter is larger for strongly absorbing media.

The present analysis aims at (1) gaining a physical understanding of transient radiation transfer in participating media, (2) performing a parametric study for the time-dependent hemispherical reflectance of a cold plane-parallel slab of an absorbing and isotropically scattering medium subject to a collimated Gaussian pulse, and (3) developing simple correlations for the maximum of the time-resolved hemispherical reflectance. The study pays particular attention to the maximum transient hemispherical reflectance which can easily be measured experimentally using a time-resolved attenuated total reflectance device [4]. Reflectance is preferred to transmittance as its magnitude and the associated signal to noise ratio are much larger, without requiring a powerful radiation source that could heat up or damage the samples. This issue is of particular concern for non-invasive in vivo sensing of biological tissues.

2 CURRENT STATE OF KNOWLEDGE

Due to the challenges encountered in solving the RTE several simplifying approaches have been suggested. First, the diffusion approximation has been used extensively in biomedical applications [4]. Its major advantage resides in the fact that there exist analytical solutions for the time-resolved hemispherical reflectance for simple geometries [4]. Brewster and Yamada [5] used the Monte Carlo method to study the effects of single scattering albedo, optical thickness, anisotropic scattering, and detector field of view on time-resolved transmittance and reflectance of an optically thick slab subjected to a picosecond collimated pulse. The numerical results were in good agreement with predictions of the diffusion approximation at long times [5]. Brewster and Yamada propose to use their findings to retrieve the radiation characteristics of absorbing and scattering media from transient transmission measurements at long times. However, their study also indicates that the diffusion theory predictions can be poor at early times, including the maximum hemispherical reflectance and the time at which it occurs. Other studies have shown that the diffusion approximation fails to predict the transmittance at early times for all optical thicknesses and also at long times for optically thin slabs [6]. In addition, Guo *et al.* [7] showed that the diffusion approximation fails for both collimated radiation and strong anisotropically scattering media.

Moreover, analytical solutions of the transient RTE in homogeneous, isotropically scattering plane-parallel slab having a non-reflecting front surface with a

blackbody back surface exposed to a collimated source have been obtained by Pomraning [8]. Also, Wu [9] used analytical solutions to obtain expressions for the hemispherical transmittance and reflectance. In addition, Wu [9] used the integral equation to compute the temporal reflectance and transmittance of 1-D absorbing and isotropically scattering slabs with various scattering albedos and optical thicknesses that compared well with results obtained using the Monte Carlo method. Tan and Hsu [10] used an integral formulation to simulate radiative transport in a 1-D plane-parallel slab of a homogeneous absorbing and isotropically scattering medium with a black back surface exposed to diffuse or collimated irradiation. The authors then extended the method to solve the same problem in three-dimensional geometries [11].

Numerical techniques have also been used to solve the transient RTE. First, in a series of papers, Kumar and co-workers solved the transient radiation transfer equation for different geometries, scattering characteristics, and boundary conditions using various methods, including the P_1 approximation [12], Monte Carlo [13–15], discrete-ordinates [6, 16, 17], and radiation element [18] methods and compared their results with predictions based on other methods or approximations [19] or with experimental data [17]. Moreover, Hsu [15] used the Monte Carlo method to study the effect of various parameters on the radiation transfer through a one-dimensional, plane-parallel, cold, absorbing, and isotropically scattering medium. The author focused on the transient local fluence within the slab by accounting for specular internal reflection at the slab surfaces. Elaloufi *et al.* [6] used a conventional discrete ordinate method (DOM) to solve the transient RTE and assess the validity of the diffusion approximation for slabs with different radiation characteristics and anisotropy. Also, Ayranci *et al.* [20] used the method of lines solution of the DOM to predict transmittance of a cubical enclosure of purely scattering media. Recently, Chai *et al.* [21] used the Finite Volume Method to simulate transient radiation transfer in a cube of absorbing and isotropically scattering medium with different boundary conditions and compared the results with published ones. On the other hand, Boulanger and Charette [22] used the DOM coupled with the piecewise parabolic advection (PPA) scheme to solve the transient multidimensional RTE for a collimated light pulse propagating in a semi-infinite, semi-transparent, non-homogeneous medium. Finally, Lu and Hsu [23] have developed the reverse Monte Carlo method in order to reduce the excessive computational time of the conventional Monte Carlo method and applied it to various geometries and scattering media. Similarly, Katika and Pilon [24] have developed the modified method of characteristics used in the present study. Advantages of this method versus other methods include its use for solving coupled equations using other numerical schemes, and its ability to capture the sharp discontinuities associated with the propagation of a radiation front in transient radiation transport.

Unfortunately, it was not possible to obtain analytical expressions [8,9] for the

maximum reflectance and the time at which it occurs. Instead, a numerical parametric study is performed using the modified method of characteristics and discussed in the following sections.

3 ANALYSIS

Let us consider transient radiation transfer in a homogeneous absorbing and isotropically scattering but non-emitting plane-parallel slab of thickness L as shown in Figure 1. The front surface of the slab ($z = 0$) is exposed to a normally collimated and monochromatic incident Gaussian pulse. The index of refraction of the slab is assumed to be identical to that of the surroundings and equal to unity. Thus, the entire incident light is transmitted through the front surface and internal reflection can be ignored. The back surface of the slab ($z = L$) is treated as black and cold. This can be implemented by coating the surface with paints or soot particles depending on the wavelength of interest. Finally, a Gaussian pulse is considered instead of other pulse shapes as it closely matches the shape produced by lasers or light emitting diodes.

3.1 Governing Equation

To solve the one-dimensional radiative transfer equation for collimated irradiation, the intensity is split into two parts: (i) the radiation scattered from the collimated radiation source and (ii) the remaining collimated beam after partial extinction by absorption and scattering along its path. The contribution from emission by the medium is negligible compared to the incident and scattered intensities, and consequently the medium can be considered as cold. Thus, the intensity for a gray medium is written as $I(z, \mu, t) = I_c(z, \mu, t) + I_d(z, \mu, t)$. The collimated intensity $I_c(z, \mu, t)$ at location z and time t in direction μ, remnant of any incident irradiation $I_i(t)$, is given by [2, 8], $I_c(z, \mu, t) = I_i(t - z/c)\delta(\mu - \mu_0)e^{-\beta z}$ where $\delta(\mu - \mu_0)$ is the Dirac's delta function and, in the present case, the incident direction μ_0 corresponds to the normal direction, i.e., $\mu_0 = 1$. Thus, the governing equation for the diffuse radiation intensity $I_d(z, \mu, t)$ along the characteristics curves of the photons [2, 25] can be written as,

$$\frac{1}{c}\frac{\mathrm{D}I_d(z,\mu,t)}{\mathrm{D}t} = -\beta I_d(z,\mu,t) + \frac{\sigma_s}{4\pi}\int_{4\pi} I_d(z,\mu_i,t)\mathrm{d}\Omega_i + \frac{\sigma_s}{4\pi}I_i(t - z/c)e^{-\beta z}H(t - z/c) \quad (2)$$

where DI_d/Dt is the total derivative of $I_d(z, \mu, t)$ along the characteristic curves $\mathrm{d}z/\mathrm{d}t = c\mu$.

3.2 Initial and Boundary Conditions

In order to solve the above governing equation, initial and boundary conditions must be specified. First, the initial intensity at all locations and in all directions at time $t = 0$ is taken as zero. At subsequent times, the radiation intensity incident on the front face (at $z = 0$) is a truncated Gaussian distribution with a pulse width t_p expressed as,

$$I_i(t) = I_0 \exp\left[-4\ln 2\left(\frac{t - t_c}{t_p}\right)^2\right], 0 < t < 2t_c \text{ and } I_i(t) = 0, t \geq 2t_c \quad (3)$$

In the present study, $I_i(t)$ reaches its maximum value I_0 at time $t_c = 3t_p$.

Finally, for the diffuse component, I_d, the front is transparent while the back surface is assumed to be black and cold, i.e., $I_d(z = 0, \mu > 0, t) = 0$ and $I_d(z = L, \mu < 0, t) = 0$. The value of the diffuse intensity $I_d(z = 0, \mu < 0, t)$ and $I_d(z = L, \mu > 0, t)$ need not be considered, because the method of solution uses boundary conditions only for intensity entering the computational domain [25].

3.3 Dimensional Analysis

Dimensional analysis of the RTE can be performed by defining the following independent dimensionless variables, $z^* = z/L$, $I^* = I/I_0$, and $t^* = t/1/\beta c = \beta ct$ where L is the slab thickness, I_0 is the maximum value reached by the time-dependent incident intensity, and $1/\beta c$ represents a characteristic time for radiation propagation through the slab. Substituting the dimensionless parameters in Equation (1) for one-dimensional transient radiation transfer problems along the z-direction yields,

$$\frac{\partial I^*}{\partial t^*} + \frac{\mu}{\beta L}\frac{\partial I^*}{\partial z^*} = -I^* + \frac{\omega}{4\pi}\int_{4\pi} I^*(\hat{\mathbf{s}}_i)\Phi(\hat{\mathbf{s}}_i, \hat{\mathbf{s}})\mathrm{d}\Omega_i \quad (4)$$

where ω is the single scattering albedo defined as $\sigma_s/(\kappa + \sigma_s)$. One can also recognize the optical thickness βL. Thus, the dimensionless intensity I^* at time t^* and location z^* in direction μ depends on the dimensionless variables ω, βL, and Φ, i.e., $I^* = I^*(z^*, \mu, t^*, \omega, \beta L, \Phi)$. After solving for the intensity in all directions at every time and location, the time-resolved transient hemispherical reflectance $R(t^*)$ at the front surface ($z^* = 0$) can be computed based

on the following definition,

$$R = -2\pi \int_{-1}^{0} I^*(0, \mu, t^*, \omega, \beta L, \Phi)\mu \mathrm{d}\mu = R(t^*, \omega, \beta L, \Phi) \tag{5}$$

Furthermore, if the medium is isotropically scattering, i.e., $\Phi(\hat{\mathbf{s}}_i, \hat{\mathbf{s}}) = 1$, the transient hemispherical reflectance of the slab is a function of only three dimensionless numbers, i.e., $R = R(\beta ct, \omega, \beta L)$. Note that other characteristic times could have been selected such as: (1) the pulse width t_p, (2) the time at which the incident intensity reaches its maximum t_c, (3) the time for the pulse to travel ballistically through the slab given by L/c, or (4) the characteristic time of the scattering process alone defined as $t^* = \sigma_s ct$. In all cases, ω, βL and Φ appear as relevant dimensionless parameters. In addition, the dimensionless quantities βct_p and βct_c appear when time is scaled with t_p and t_c, respectively.

3.4 Method of Solution

The governing Equation (2) and the associated boundary conditions are solved using the modified method of characteristics [25]. Extensive discussion of this method for both transient and steady-state radiation transfer has been previously reported [24, 26] and need not be repeated here. Comparison between numerical integral solutions [9] and the modified method of characteristics were found to be in good agreement with a mean error of less than 5% for $\beta L = 0.5$ and $\omega = 0.05$ and 0.95 [25]. The same accuracy is expected in the present results. A uniform discretization of N_z points along the $z-$direction and N_θ discrete directions for θ varying from 0 to π was used. The time interval Δt had little effect on the numerical results as long as it satisfied $\Delta t \leq \Delta z/c$. Thus, Δt was set equal to $\Delta z/c$ where $\Delta z = L/(N_z - 1)$. After solving for the intensities in the discrete directions at every point, the hemispherical reflectance R of the slab was computed from Equation (5).

4 RESULTS AND DISCUSSION

A large range of optical thickness ($0 \leq \beta L \leq 50$), single scattering albedo ($0.05 \leq \omega \leq 1$), and incident pulse width ($0.015 \leq \beta ct_p \leq 0.15$) have been explored. The number of discrete points N_z and directions N_θ were varied between 100 and 2000 and between 50 and 450, respectively to obtain converged numerical solutions for each pair of parameters βL and ω. In all cases, the results were assumed to be numerically converged when doubling both N_z and

N_θ produced less than 1% change in the value of the computed reflectance. The integrals in Equations (2) and (5) were computed using the 3/8 Simpson's rule [27]. The CPU time taken for computing the transient hemispherical reflectance for the case of $\beta L = 0.5$ and $\omega = 0.95$, for example, using a spatial discretization of $N_z = 101$ points and an angular discretization of $N_\theta = 25$ directions per octant was about 21 seconds on a 512 MHz Pentium III for a total dimensionless time of t^* $(=\beta ct) = 8$.

4.1 Effect of βL and ω

Figure 2 shows the typical transient hemispherical reflectance of the plane-parallel slab with either black or specularly reflecting back surface as a function of βct, for $\omega = 0.7$, $\beta L = 0.5$, and $\beta ct_p = 0.15$. Since there is no direct reflection of the incident beam from the front surface, the reflected signal is due to back scattering of the incident radiation by the slab. The maximum value of the reflectance is denoted by R_1 and occurs at dimensionless time βct_1. For a black back surface, the reflectance reveals only one maximum as the pulse is absorbed once it reaches the back of the slab. On the other hand, for a specularly reflecting back surface, two maxima are evident. The first one is identical to that observed with a black back surface. The second maximum corresponds to radiation emerging from the slab after being reflected by the back surface.

Moreover, Figure 3 shows the transient hemispherical reflectance as a function of the dimensionless time t^* for different values of the single scattering albedo ω and for $\beta L = 0.7$ and $\beta ct_p = 0.15$. Similar plots have been obtained for other values of βL. One can see that the hemispherical reflectance R increases as ω increases for any given dimensionless time βct. This can be attributed to the increase in the scattering coefficient resulting in a larger fraction of the incident intensity being back-scattered by the medium. It is also worth noting that the dimensionless time βct_1 appears to be independent of ω and is equal to 0.6 in these cases.

Finally, Figure 4 shows the transient hemispherical reflectance as a function of the dimensionless time βct for different values of βL and for $\omega = 0.95$ and $\beta ct_p = 0.15$. Similar results have been obtained for different values of ω. Figure 4 indicates that the maximum reflectance R_1 increases with βL up to a critical optical thickness $(\beta L)_{cr}$ beyond which it is independent of βL. The highest value for the maximum reflectance is denoted $R_{1,max}$. One can also note that $(\beta L)_{cr}$ for this case is equal to 0.15 which, coincidentally, is also the value of βct_p. The effect of the incident pulse width, βct_p, will be discussed in detail in Section 4.3.

4.2 Maximum Reflectance

Let us now focus our attention to the value of the maximum reflectance R_1 and its occurrence at time βct_1 as functions of the optical thickness βL and of the single scattering albedo ω. Figure 5 (top) shows the peak value of the transient reflectance R_1 as a function of the optical thickness βL ranging from 0.01 to 50 for $\beta ct_p = 0.15$ and for four different values of the single scattering albedo between 0.05 and 1. It also shows (bottom) the corresponding values of βct_1 as a function of βL for values up to 1 for the sake of clarity. The error bars correspond to a numerical uncertainty of $\pm 5\%$. It is interesting to note that the critical optical thickness $(\beta L)_{cr}$ is identical for R_1 and for βct_1. Moreover, an optically thin and optically thick regimes can be identified as follows:
Optically Thin Regime, $\beta L \leq (\beta L)_{cr}$. In this regime, R_1 varies linearly with $\ln(\beta L)$ and increases as ω increases. On the other hand, βct_1 is nearly independent of ω and varies linearly with βL. In addition, $(\beta L)_{cr}$ depends on the pulse width βct_p.
Optically Thick Regime, $\beta L > (\beta L)_{cr}$. In this regime, R_1 is independent of βL but increases with ω. However, βct_1 appears to be independent of both βL and ω. Beyond the critical value $(\beta L)_{cr}$, the optical thickness βL has no effect on the maximum reflectance, and R_1 and βct_1 reach their maximum denoted by $R_{1,max}$ and $\beta ct_{1,max}$, respectively.

4.3 Effect of the Incident Pulse Width

To investigate the effect of the dimensionless pulse width on the hemispherical reflectance, different values of βct_p have been investigated, namely 0.15, 0.075, and 0.015. Figure 6 plots R_1 versus βL for different values of βct_p at $\omega = 0.7$. One can see that R_1 increases as βct_p increases for fixed values of ω and βL. This can be attributed to the fact that increasing the pulse width increases the radiant energy in the slab at any given time and therefore, increases the scattered radiation intensity and the hemispherical reflectance.

In addition, Figure 7 shows the ratio $\beta ct_1/\beta ct_p$ and R_1 as functions of βL for different values of the single scattering albedo ω. It indicates that as βL tends to zero, t_1 tends asymptotically toward $3t_p$. Moreover, βct_1 is independent of ω in the optically thin regime for all values of βct_p. Additionally, once βL reaches βct_p, the value of βct_1 and R_1 become independent of βL. This is defined as the optically thick regime because increasing βL no longer has any effect on the values of βct_1 and R_1. In the optically thick regime $\beta ct_1 = \beta ct_{1,max}$ and $R_1 = R_{1,max}$.

Finally, for each value of ω, the values of $(\beta L)_{cr}$ can be obtained from R_1 versus

βL or from βct_1 versus βL. The values of $(\beta L)_{cr}$ vary within 5% when obtained from either R_1 or βct_1. Figure 8 shows the average critical optical thickness $(\beta L)_{cr}$ as a function of the dimensionless pulse width βct_p for different values of ω. One can see that for $\beta ct_p = 0.015$ and 0.075, the average value of the critical optical thickness $(\beta L)_{cr}$ is approximately βct_p. However, when βct_p increases to 0.15, the average value of $(\beta L)_{cr}$ falls below βct_p possibly due to numerical error. Nonetheless, this finding indicates that $(\beta L)_{cr}$ is equal to βct_p within 10%.

4.4 Correlations

Developing correlations for transient hemispherical reflectance could be useful as a simple method for retrieving the optical thickness and the single scattering albedo of a substance. Then, each regime features its own set of correlations for R_1 and βct_1.

Optically Thin Regime, $\beta L \leq \beta ct_p$. In this regime the maximum reflectance R_1 varies as a function of $\ln(\beta L)$ as indicated by Figures 5 and 6 and can be expressed as,

$$R_1(\omega, \beta ct_p, \beta L) = C_1 \ln(\beta L) + C_2 \tag{6}$$

where the slope $C_1 = C_1(\omega, \beta ct_p)$ and the constant $C_2 = C_2(\omega, \beta ct_p)$ depend on both the single scattering albedo and the dimensionless pulse width. Figure 9 illustrates $C_1/\beta ct_p$ and $C_2/\omega\beta ct_p$ as functions of ω and βct_p, respectively for $\beta L \leq \beta ct_p$. It shows that both C_1 and C_2 vary with $\omega\beta ct_p$ according to,

$$C_1 = 0.05\omega\beta ct_p = 0.05\sigma_s ct_p \tag{7}$$
$$C_2 = (-0.8\beta ct_p + 0.375)\sigma_s ct_p \tag{8}$$

This confirms the finding that if the slab is non-scattering ($\sigma_s = 0$) its reflectance vanishes. The coefficients of regression R^2 for C_1 and C_2 are 0.998 and 0.973, respectively.

Similarly, Figure 7 indicates that, within the numerical uncertainty,

$$\beta ct_1 = 3\beta ct_p + \beta L \qquad \text{for } \beta L < \beta ct_p \tag{9}$$

The value of $\beta ct_1 = 3\beta ct_p$ for the limiting case when βL approaches 0 can be explained from first principles. Indeed, the scattered intensity in direction $\hat{\mathbf{s}}$ from a ray of radiation propagating in direction $\hat{\mathbf{s}}_i$ by an infinitesimally thin

element dL can be expressed as [2],

$$dI_{sca}(\hat{\mathbf{s}},t) = \frac{\sigma_s dL}{4\pi}\int_{4\pi} I(\hat{\mathbf{s}}_i,t)\Phi(\hat{\mathbf{s}}_i,\hat{\mathbf{s}})\mathrm{d}\Omega_i \tag{10}$$

when βL approaches 0, one can safely assume that single scattering prevails [28]. Then, the incoming intensity from direction $\hat{\mathbf{s}}_i$ is identical to the incident intensity, i.e., $I(\hat{\mathbf{s}}_i,t) = I_i(t)\delta(\hat{\mathbf{s}}-\hat{\mathbf{s}}_0)$ and Equation (10) reduces to, $I(\hat{\mathbf{s}},t) = \frac{\sigma_s L}{4\pi} I_i(t)\Phi(\hat{\mathbf{s}}_0,\hat{\mathbf{s}})$. Then, using Equation (5) for an isotropically scattering slab, the hemispherical reflectance simplifies to,

$$R(t) = \frac{\sigma_s L}{2}\frac{I_i(t)}{I_0} \tag{11}$$

Thus, the reflectance $R(t)$ is maximum when $I_i(t)$ is maximum, that is, when $t = t_c = 3t_p$, in our case. Moreover, predictions from Equation (11) compare well with numerical results for $\beta L = 0.0001$ and $\beta c t_p = 0.015$. The maximum reflectance was $R_1 = 0.005\%$ and occurred at $\beta c t_1 = 0.0452$, with a relative error of 5.5% with respect to the predictions of Equation (11).

Optically Thick Regime, $\beta L > \beta c t_p$. In this regime, the maximum reflectance $R_{1,max}$ and $\beta c t_{1,max}$ is independent of βL. Figure 10 shows the linear increase of the ratio $R_{1,max}/\beta c t_p$ as a function of ω. It also shows that $\beta c t_{1,max}$ as a function of $\beta c t_p$ for all values of βL and ω in this regime. It establishes that,

$$R_{1,max} = 0.156\sigma_s c t_p \qquad \text{for } \beta L > \beta c t_p \tag{12}$$

$$\beta c t_{1,max} = 4\beta c t_p \qquad \text{for } \beta L > \beta c t_p \tag{13}$$

4.5 Discussion

First, numerical simulations were performed for different indices of refraction ($n = 1$, 1.33, and 1.5) for $\omega = 0.7$ and $\beta L = 0.5$ while still neglecting internal reflectance. This practically can be achieved by immersing the device in an index matching fluid whose index of refraction is the same as that of the slab to be analyzed. As expected from dimensional analysis, the same values of the transient hemispherical reflectance shown in Figure 3 were obtained for the same set of parameters $(\omega, \beta L, \beta c t_p)$.

Moreover, Figure 11 compares the predictions of the above correlations with numerically computed values of R_1 and $\beta c t_1$, respectively. The computed maximum hemispherical reflectance is properly predicted within a maximum absolute error of $\pm 0.21\%$, and every numerically computed dimensionless time

βct_1 is predicted within a maximum absolute error of ± 0.025. The maximum relative error was determined for small values of R_1 that might be difficult to measure experimentally.

Additionally, the above correlations were validated against numerical results reported by Wu [9]. In particular Figures 3, 9 and 10 in Ref. [9] were digitized and the maximum reflectance was retrieved using digiXY. The optical thickness βL ranged from 0.25 to 16, the single scattering albedo ω ranged from 0.05 to 1, and the dimensionless pulse width was either 0.15 or 0.3333 [29] while $t_c/t_p = 3$. Most data fell in the optically thick regime. The single scattering albedo was retrieved within 5% of its input value by recognizing that $\omega = 4R_{1,max}/0.156\beta ct_{1,max}$. If one assumes that t_c, t_p, $t_{1,max}$ and $R_{1,max}$ are accessible experimentally, the scattering coefficient σ_s can be found from Equation (12) within 16% of its input value. Moreover, we verified that $t_{1,max} = t_p/4$ within 11%.

Finally, the above correlations could be used to determine the radiation characteristics of homogeneous absorbing and isotropically scattering media by experimentally measuring the maximum of the transient reflectance for slabs having at least two different thicknesses or by holding $t_c = 3t_p$ and varying the pulse width of the incident radiation. The slab thickness or the pulse width must be chosen in such a way to cover both the optically thin and thick regimes. Note that this bears some analogy with the method proposed by Yamada and Kurosaki [3] to retrieve the radiation characteristics of porous materials from *steady-state* emittance measurements. Indeed, the authors assumed an isotropic scattering phase function and used the fact that the emittance of an optically thick and isotropically scattering medium is independent of the optical thickness and depends only on the single scattering albedo. Alternatively, the method could also serve to obtain an initial guess for more complex inversion schemes accounting for anisotropic scattering.

5 CONCLUSIONS

This paper proposes a method to determine the radiation characteristics of homogeneous, cold, absorbing and isotropically scattering plane-parallel slab with a transparent front surface and a black back surface from measured time-resolved hemispherical reflectance. It presents a parametric study focusing on the maximum hemispherical reflectance R_1 and its occurrence time βct_1. Dimensionless parameters include the optical thickness of the slab βL, the single scattering albedo ω, and the incident pulse width βct_p. Conclusions of the study are as follows: **(1)** there exist optically thin and optically thick regimes for the maximum hemispherical reflectance R_1 and the dimensionless time βct_1, **(2)** these two regimes meet at a critical optical thickness $(\beta L)_{cr}$

such that $(\beta L)_{cr} \approx \beta c t_p$, **(3)** in the optically thin regime, R_1 increases with increasing βL, ω and $\beta c t_p$, while $\beta c t_1$ is independent of ω but increases with βL such that $\beta c t_1 = 3\beta c t_p + \beta L$, **(4)** in the optically thick regime, $R_{1,max}$ is proportional to $\omega \beta c t_p$ and is independent of βL. On the other hand, $\beta c t_{1,max}$ is independent of both ω and βL such that $\beta c t_1 = 4\beta c t_p$.

Similar parametric studies could be performed for (i) other pulse shapes, (ii) independently varying t_c and t_p of the Gaussian pulse, (iii) cases when the indices of refraction across the front surface differ and one needs to account for internal reflection, and (iv) anisotropically scattering media. Similar trends and correlations are anticipated.

References

[1] S. Kumar, K. Mitra, Microscale aspects of thermal radiation transport and laser applications, Advances in Heat Transfer 33 (1999) 187–294.

[2] M. F. Modest, Radiative Heat Transfer, Academic Press, San Diego, CA, 2003.

[3] J. Yamada, Y. Kurosaki, Estimation of a radiative property of scattering and absorbing media, International Journal of Thermophysics 18 (2) (1997) 547–556.

[4] M. Patterson, B. Chance, B. Wilson, Time resolved reflectance and transmittance for the non-invasive measurement of tissue optical properties, Applied Optics 28 (12) (1989) 2331–2336.

[5] M. Q. Brewster, Y. Yamada, Optical properties of thick, turbid media from picosecond time-resolved light scattering measurements, International Journal of Heat Mass Transfer 38 (1995) 2569–2581.

[6] R. Elaloufi, R. Carminati, J. J. Greffet, Time-dependent transport through scattering media: from radiative transfer to diffusion, Journal of Optics A: Pure And Applied Optics 4 (5) (2002) S103–S108.

[7] Z. Guo, K. Kim, Ultrafast-laser-radiation transfer in heterogeneous tissues with the discrete-ordinates method, Applied Optics 42 (2003) 2897–2905.

[8] G. C. Pomraning, The Equations of Radiation Hydrodynamics, Pergamon Press, New York, NY, 1973.

[9] C.-Y. Wu, Propagation of scattered radiation in a participating planar medium with pulse irradiation, Journal of Quantitative Spectroscopy and Radiative Transfer 64 (5) (2000) 537–548.

[10] Z.-M. Tan, P.-F. Hsu, An integral formulation of transient radiative transfer, ASME Journal of Heat Transfer 123 (2001) 466–475.

[11] Z.-M. Tan, P.-F. Hsu, Transient radiative transfer in three-dimensional homogeneous and non-homogeneous participating media, Journal of Quantitative Spectroscopy and Radiative Transfer 73 (2002) 181–194.

[12] K. Mitra, M. Lai, S. Kumar, Transient radiation transport in participating media within a rectangular enclosure, Journal of Thermophysics and Heat Transfer 11 (1997) 409–414.

[13] Z. Guo, S. Kumar, K.-C. San, Multidimensional Monte Carlo simulation of short-pulse transport in scattering media, Journal of Thermophysics and Heat Transfer 14 (4) (2000) 504–511.

[14] Z. Guo, S. Kumar, Three-dimensional discrete ordinates method in transient radiative transfer, Journal of Thermophysics and Heat Transfer 16 (3) (2002) 289–296.

[15] P.-F. Hsu, Effects of multiple scattering and reflective boundary, Internation Journal of Thermal Sciences 40 (2001) 539–549.

[16] Z. Guo, S. Kumar, Discrete-ordinates solution of short-pulsed laser transport in two-dimensional turbid media, Applied Optics 40 (2001) 3156–3163.

[17] Z. Guo, S. Kumar, Three-dimensional discrete ordinates method in transient radiative transfer, Journal of Thermophysics and Heat Transfer 16 (2002) 289–296.

[18] Z. Guo, S. Kumar, Radiation element method for transient hyperbolic radiative transfer in plane-parallel inhomogeneous media, Numerical Heat Transfer: Part B 39 (2001) 371–387.

[19] K. Mitra, S. Kumar, Development and comparison of models for light pulse transport through scattering-absorbing media, Applied Optics 38 (1999) 188–196.

[20] I. Ayranci, N. Selçuk, MOL solution of DOM for transient radiative transfer in 3-D scattering media, Journal of Quantitative Spectroscopy and Radiative Transfer 84 (2004) 409–422.

[21] J. C. Chai, P.-F. Hsu, Y. Lam, Three-dimensional transient radiative transfer modeling using the finite-volume method, Journal of Quantitative Spectroscopy and Radiative Transfer 86 (2004) 299–313.

[22] J. Boulanger, A. Charette, Reconstruction optical spectroscopy using transient radiative transfer equation and pulsed laser: a numerical study, Journal of Quantitative Spectroscopy and Radiative Transfer 93 (2005) 325–336.

[23] X. Lu., P.-F. Hsu, Reverse monte carlo simulations of light pulse propagation within three-dimensional media, Journal of Thermophysics and Heat Transfer 19 (3) (2005) 353–359.

[24] L. Pilon, K. Katika, Backward method of characteristics for simulating microscale energy transport, ASME Journal of Heat Transfer 126 (2004) 735–743.

[25] K. Katika, L. Pilon, Modified method of characteristics for transient radiative transfer, Journal of Quantitative Spectroscopy and Radiative Transfer 98 (2005) 220–237.

[26] K. Katika, L. Pilon, Backward method of characteristics in radiative heat transfer, 4th International Symposium on Radiative Transfer, Istanbul, Turkey, June 18-21 (2004) 347–355.

[27] J. D. Hoffman, Numerical Methods for Engineers and Scientists, McGraw Hill, New York, NY, 1998.

[28] C. L. Tien, B. L. Drolen, Thermal radiation in particulate media with dependent and independent scattering, in Annual Review of Numerical Fluid Mechanics and Heat Transfer 1 1–32.

[29] C.-Y. Wu, Personal communication regarding Ref. [10], December 2003.

FIGURE CAPTIONS

Figure 1. Schematic of an absorbing and isotropically scattering plane-parallel slab exposed to collimated incident radiation pulse.
Figure 2. Time-resolved hemispherical reflectance R versus the dimensionless time βct for $\beta ct_p = 0.15$ with $\beta L = 0.5$ and $\omega = 0.7$ with black or specularly reflecting back surface.
Figure 3. Time-resolved hemispherical reflectance R as a function of the dimensionless time βct for different values of ω and for $\beta L = 0.7$.
Figure 4. Hemispherical reflectance R as a function of βct for different values of βL for $\omega = 0.95$ and $\beta ct_p = 0.15$.
Figure 5. Effect of the single scattering albedo ω and of the optical thickness βL on the maximum reflectance R_1 (top) and the corresponding time βct_1 (bottom) for $\beta ct_p = 0.15$.
Figure 6. Effect of the dimensionless pulse width βct_p on the maximum hemispherical reflectance R_1 for $\omega = 0.7$.
Figure 7. $\beta ct_1/\beta ct_p$ and R_1 as functions of βL and ω for (a) $\beta ct_p = 0.15$, (b) 0.075, and (c) 0.015. Error bars shown are the absolute errors.
Figure 8. Effect of the dimensionless pulse width βct_p and ω on the critical βL.
Figure 9. Value of the slope $C_1/\beta ct_p$ and constant $C_2/\sigma_s ct_p$ as a function of the single scattering albedo, ω, and the incident pulse width, βct_p, respectively, for $\beta L < \beta ct_p$.
Figure 10. Maximum hemispherical reflectance and $\beta ct_{1,max}$ scaled with βct_p, as a function of the single scattering albedo ω in the optically thick regime ($\beta L > \beta ct_p$).
Figure 11. Comparison of predicted values of the (top) R_1 and (bottom) βct_1, vs. numerically computed values for all values of βL, ω, and βct_p explored in this study.

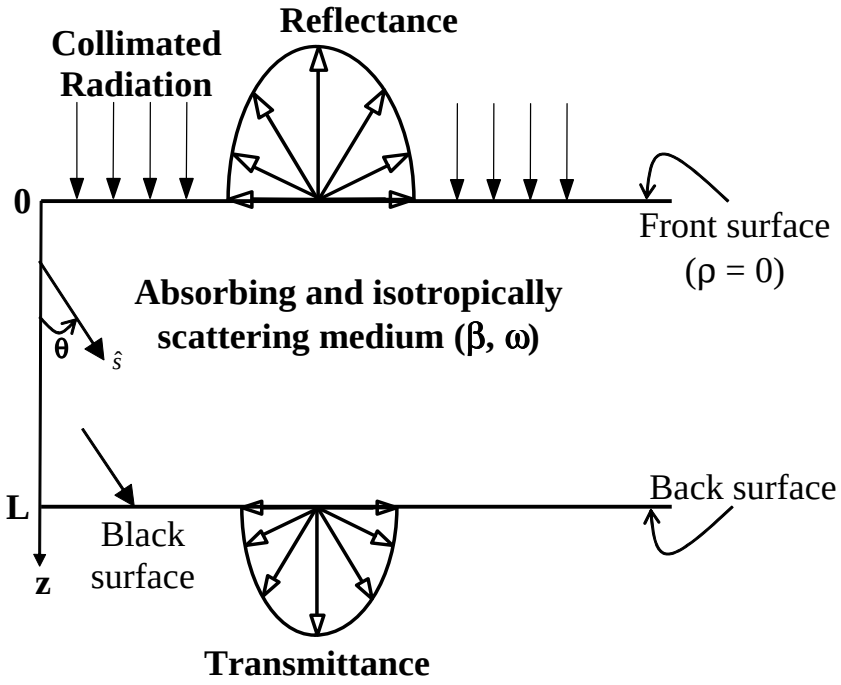

Fig. 1. Schematic of an absorbing and isotropically scattering plane-parallel slab exposed to collimated incident radiation pulse.

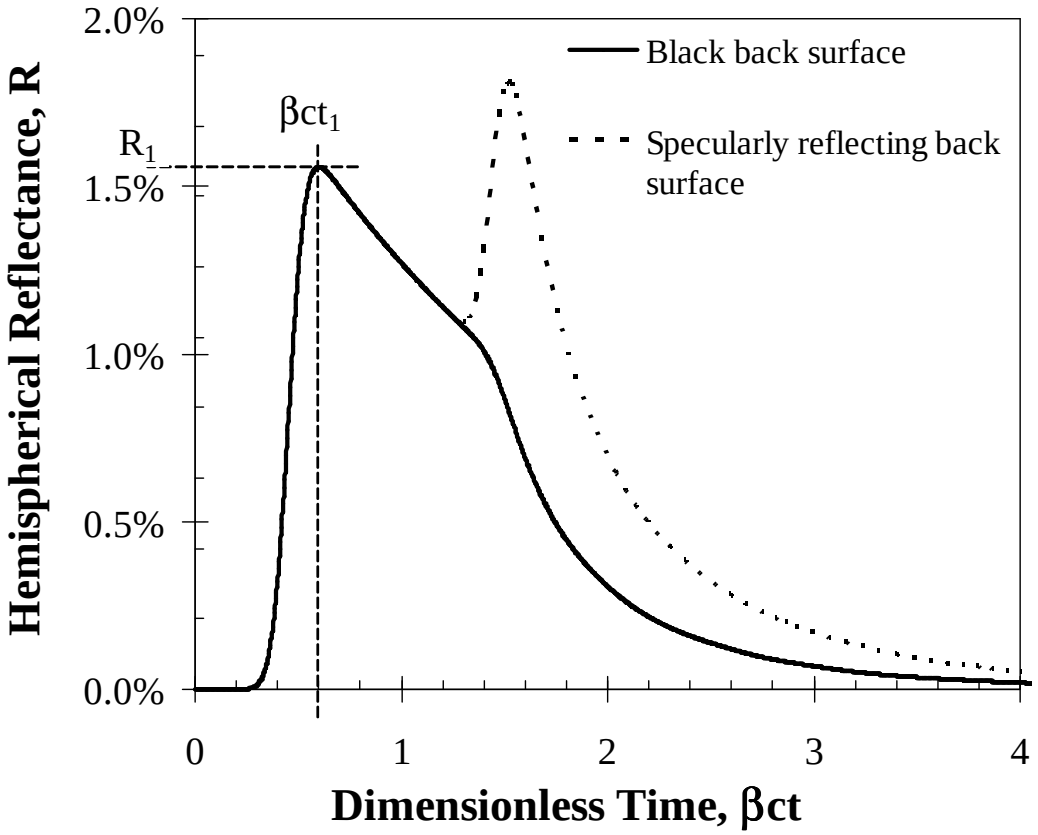

Fig. 2. Time-resolved hemispherical reflectance R as a function of the dimensionless time βct for $\beta ct_p = 0.15$ with $\beta L = 0.5$ and $\omega = 0.7$ with black or specularly reflecting back surface.

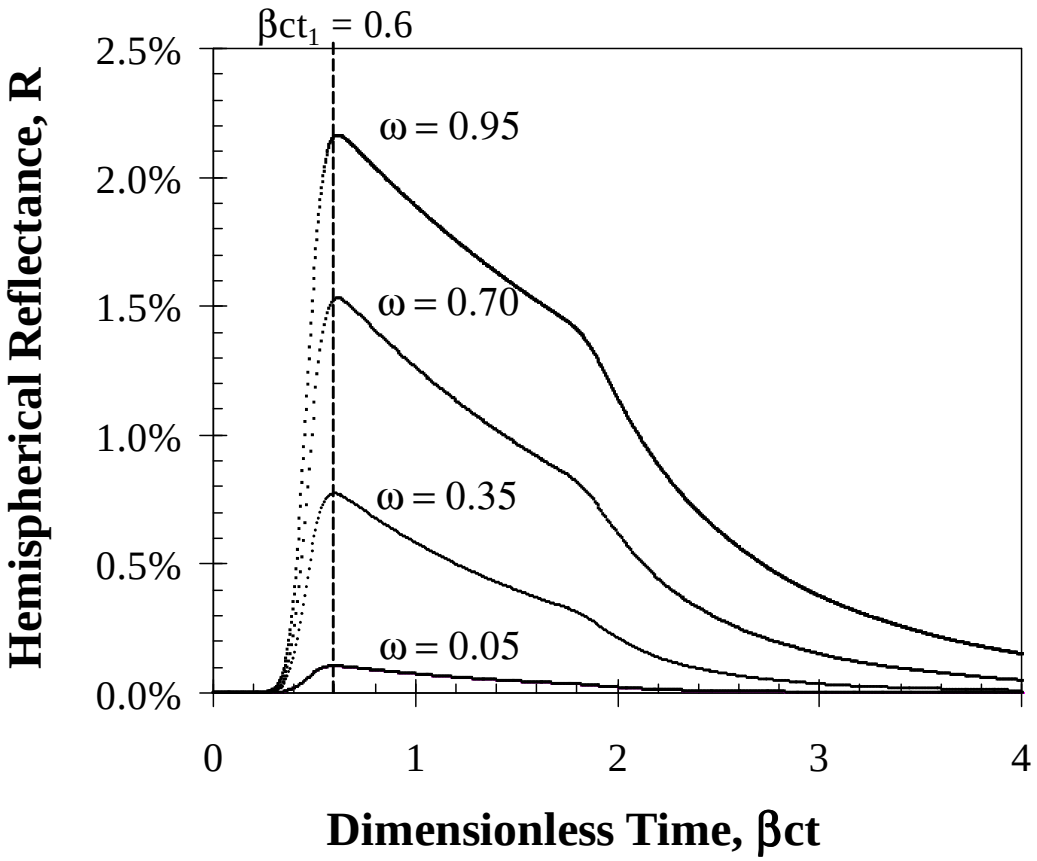

Fig. 3. Time-resolved hemispherical reflectance R as a function of the dimensionless time βct different values of ω and for $\beta L = 0.7$.

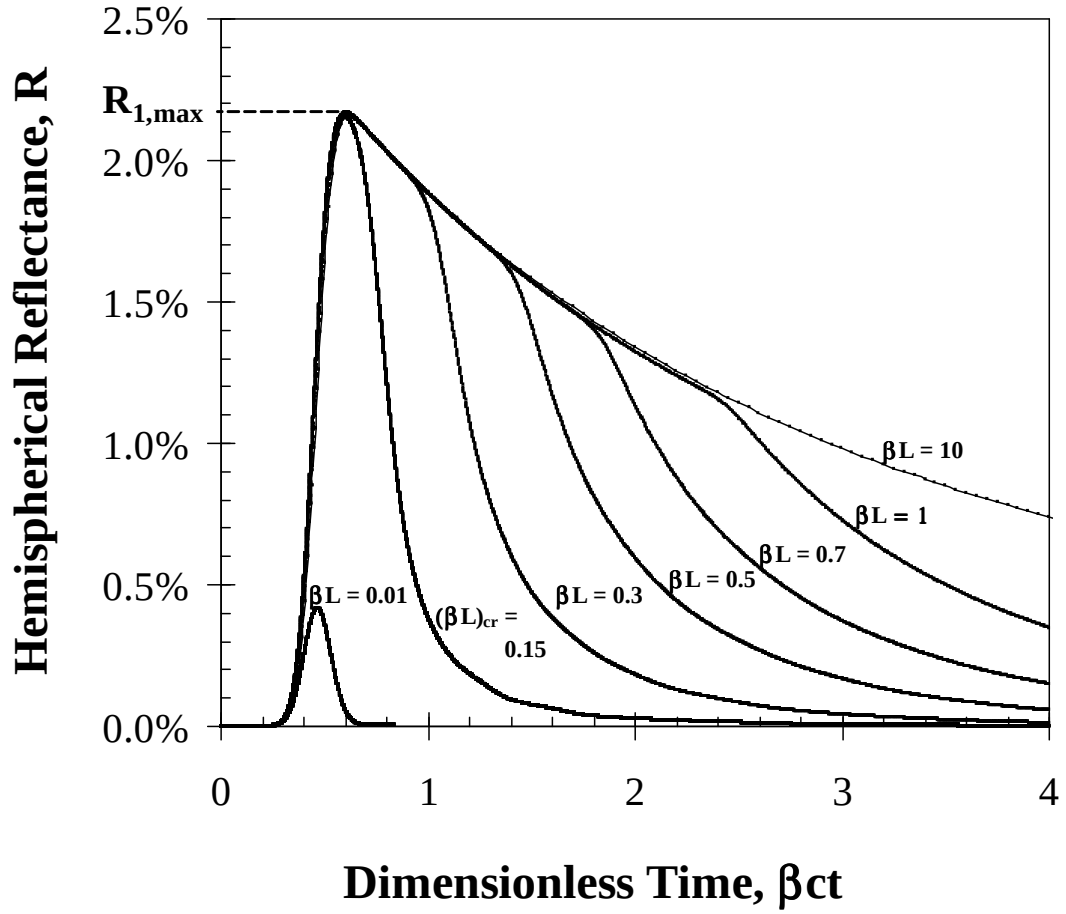

Fig. 4. Hemispherical reflectance R as a function of βct for different values of βL and for $\omega = 0.95$ and $\beta ct_p = 0.15$.

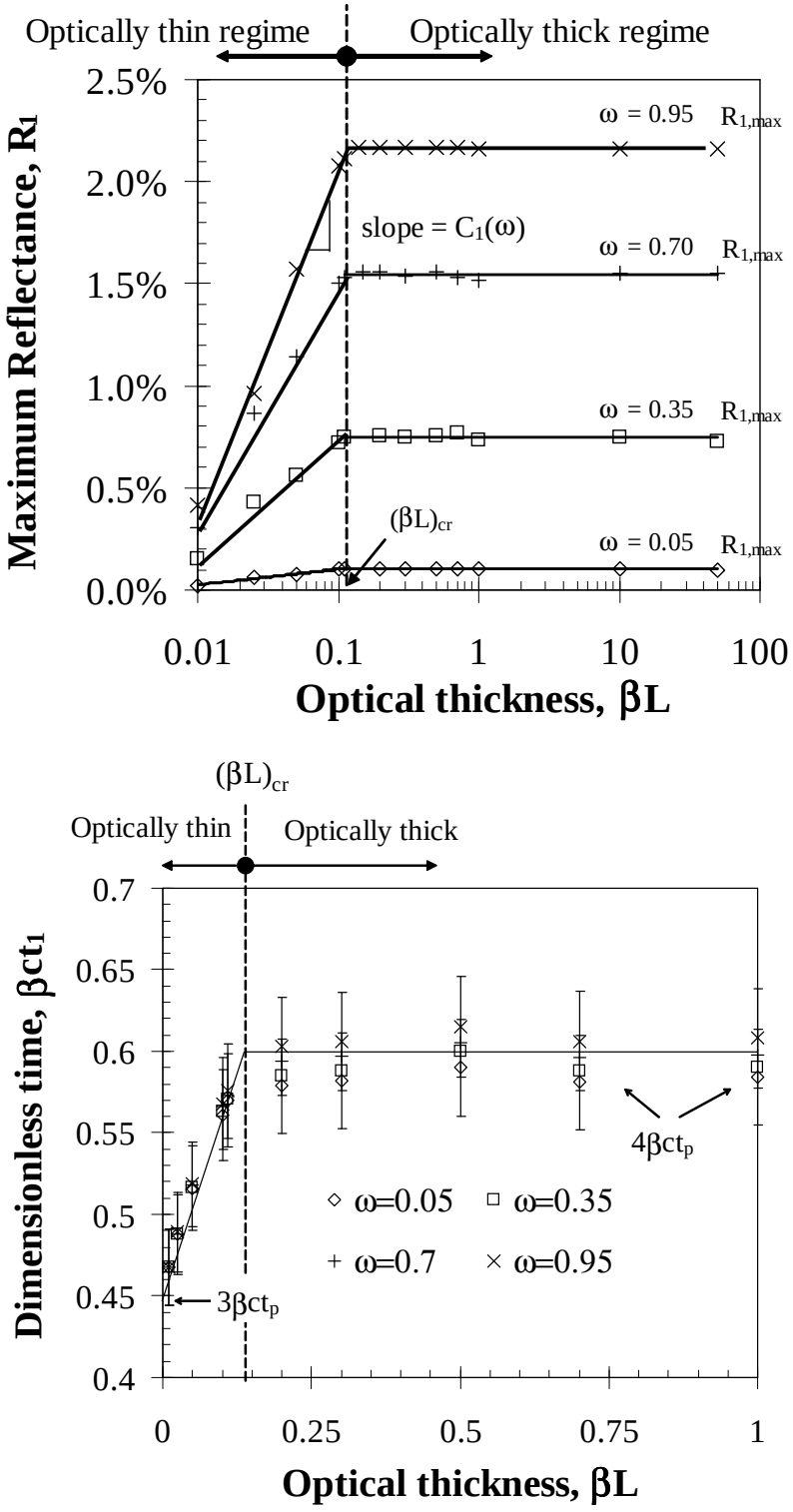

Fig. 5. Effect of the single scattering albedo ω and of the optical thickness βL on the maximum reflectance R_1 (top) and the corresponding time βct_1 (bottom) for $\beta ct_p = 0.15$.

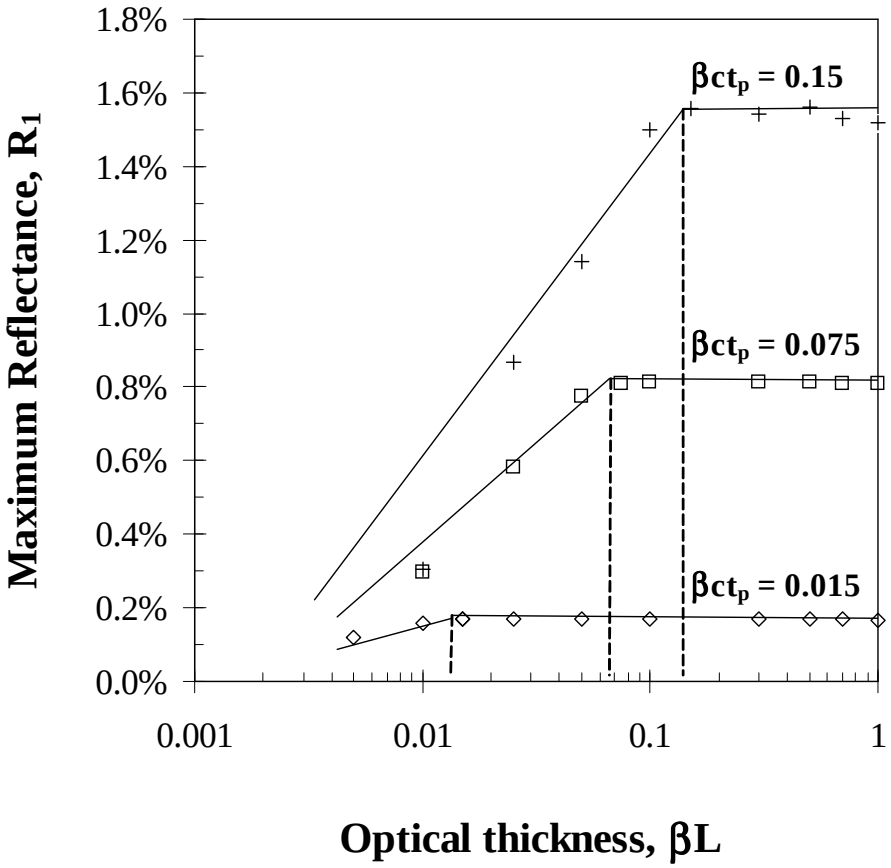

Fig. 6. Effect of the dimensionless pulse width $\beta c t_p$ on the maximum hemispherical reflectance R_1 for $\omega = 0.7$.

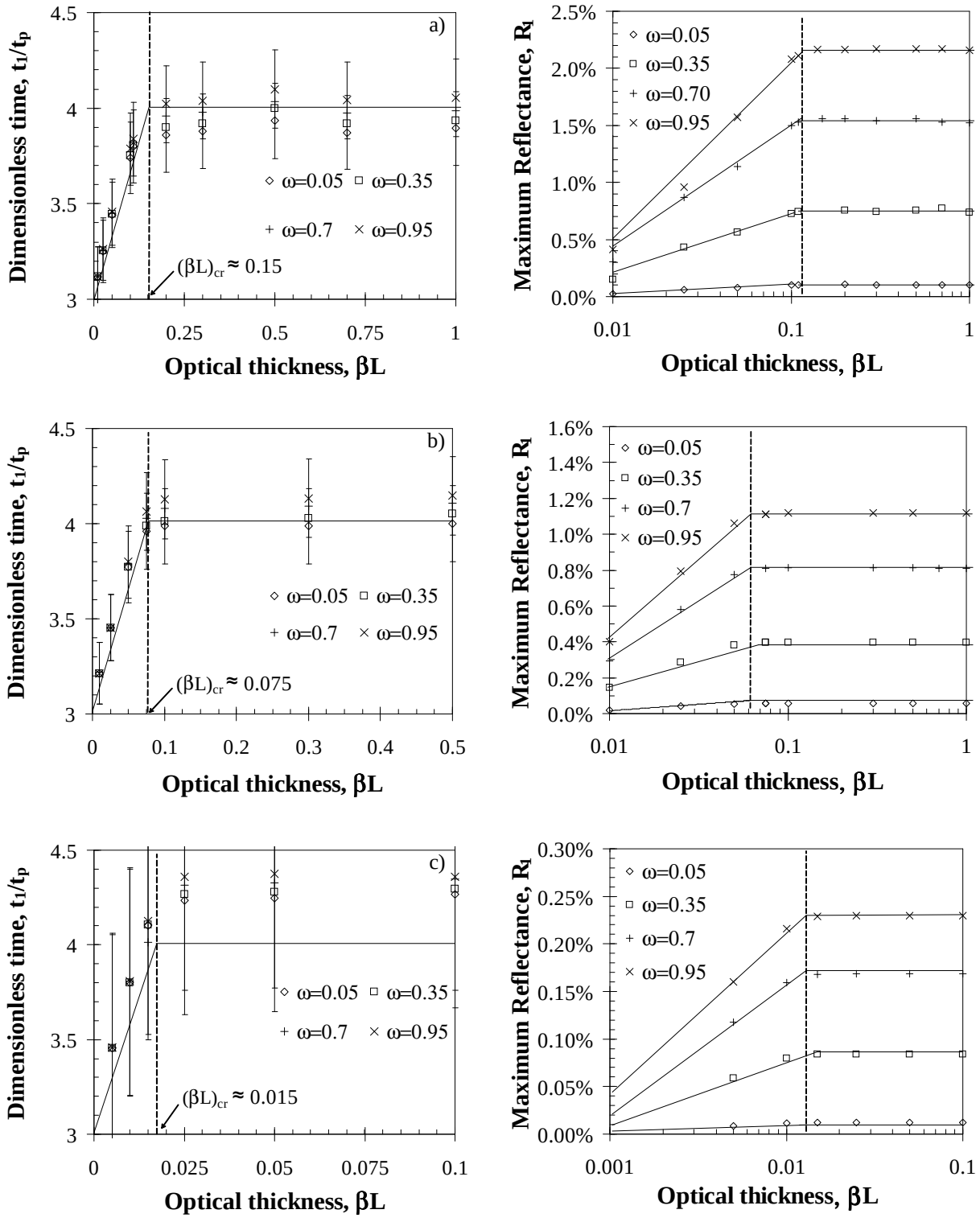

Fig. 7. $\beta ct_1/\beta ct_p$ and R_1 as functions of βL and ω for (a) $\beta ct_p = 0.15$, (b) 0.075, and (c) 0.015. Error bars shown are the absolute errors.

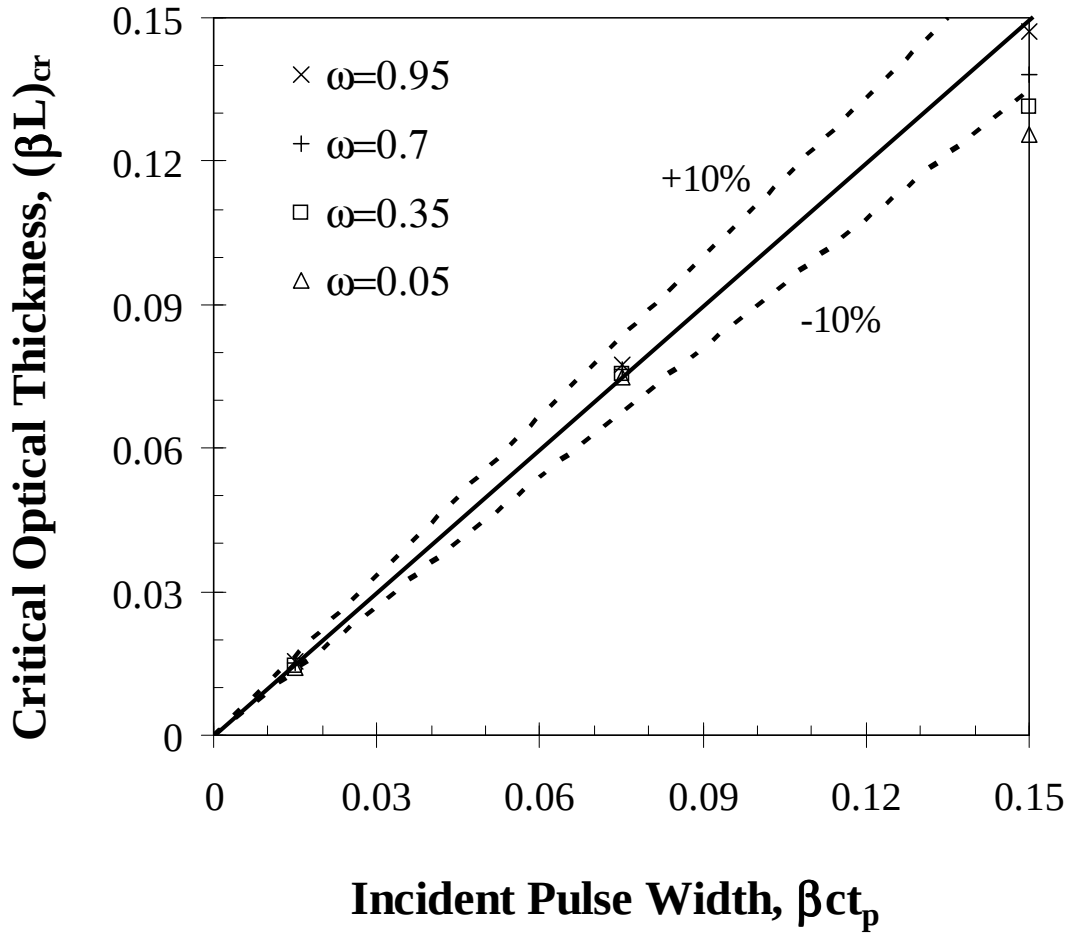

Fig. 8. Effect of the dimensionless pulse width $\beta c t_p$ and ω on the critical βL.

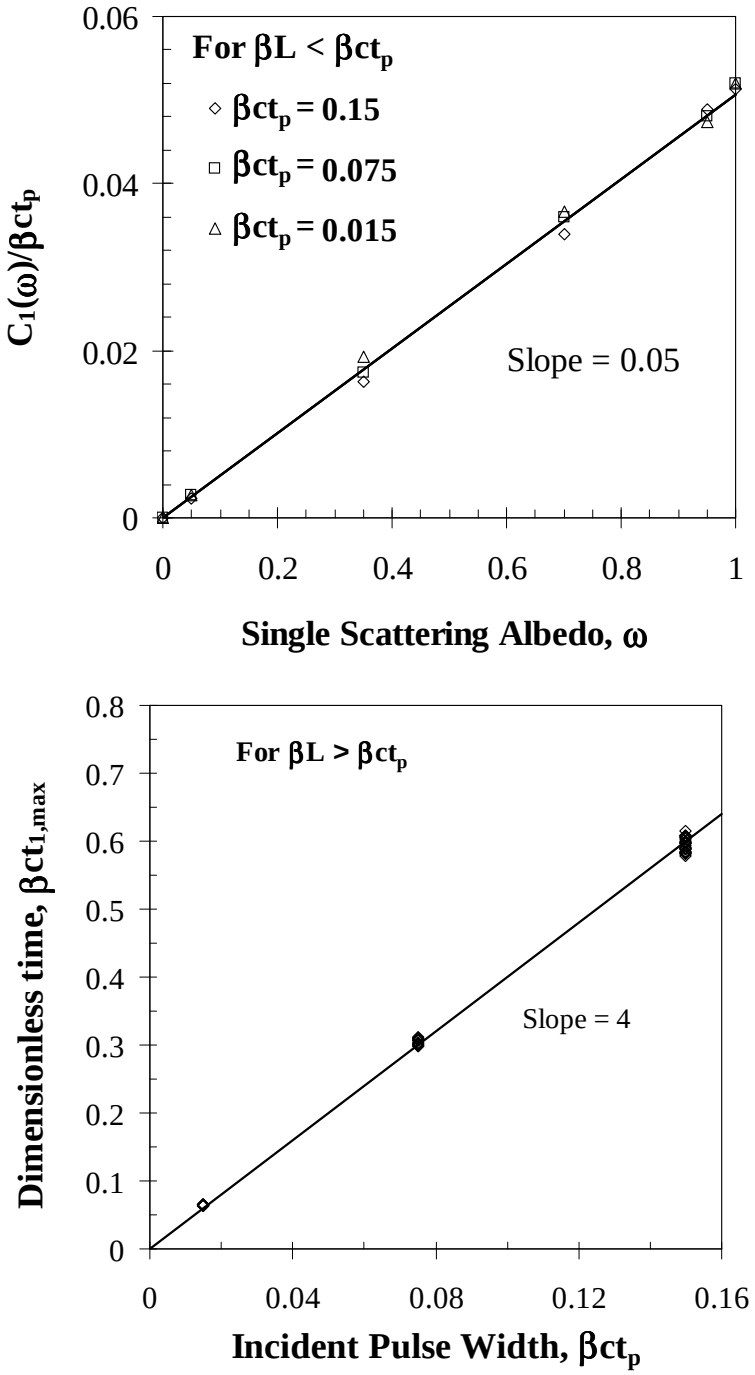

Fig. 9. Value of the slope $C_1/\beta ct_p$ and constant $C_2/\sigma_s ct_p$ as a function of the single scattering albedo, ω, and the incident pulse width, βct_p, respectively for $\beta L < \beta ct_p$.

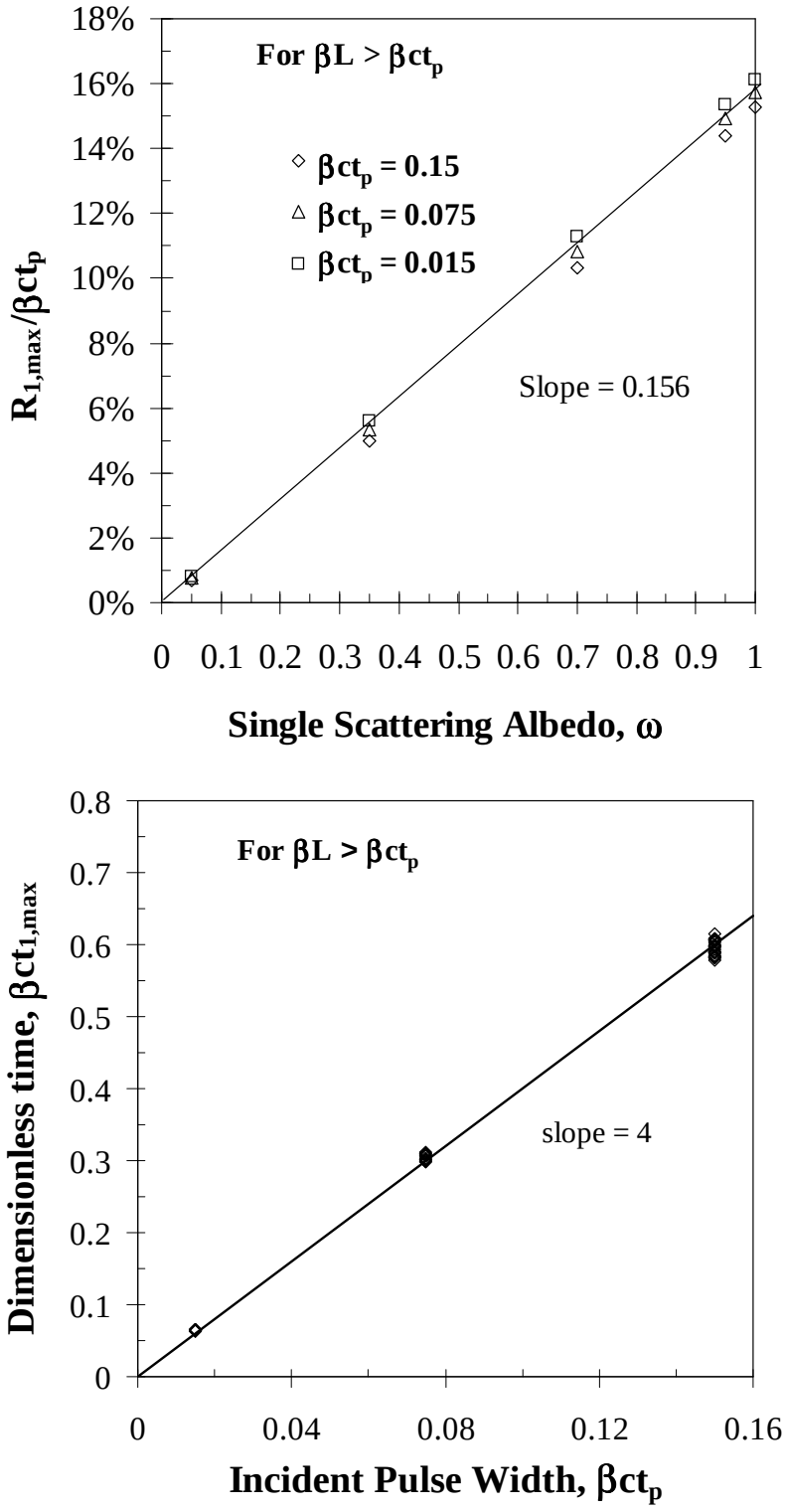

Fig. 10. Maximum hemispherical reflectance and $\beta ct_{1,max}$ scaled with βct_p, as a function of the single scattering albedo ω in the optically thick regime ($\beta L > \beta ct_p$).

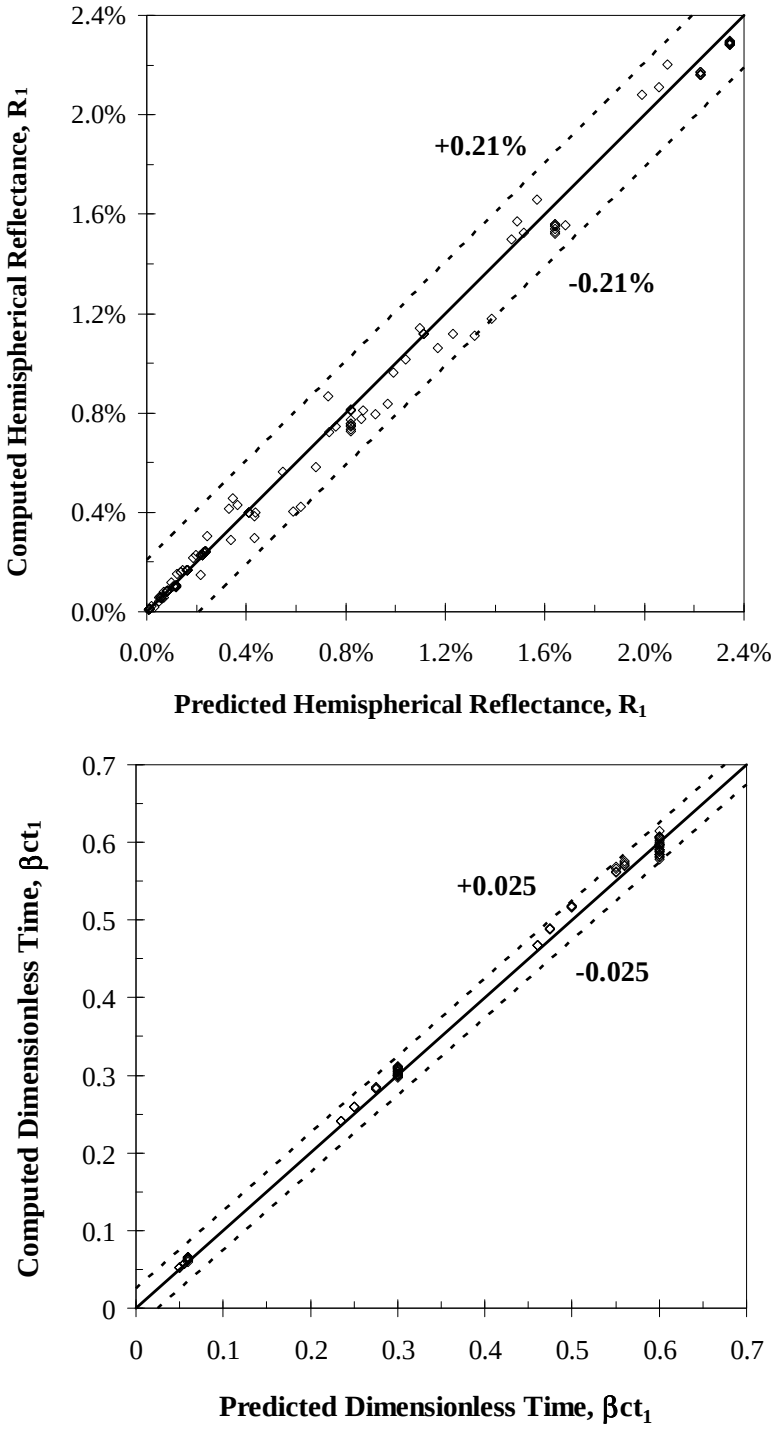

Fig. 11. Comparison of predicted values of (top) R_1 and (bottom) βct_1, vs. numerically computed values for all values of βL, ω, and βct_p explored in this study.